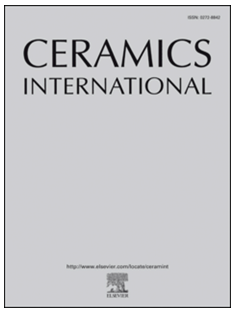

Assessment of bismuth oxide-based electrolytes for composite gas separation membranes

M. Starykevich, A. Jamale, F.M.B. Marques

PII: S0272-8842(20)32146-5

DOI: https://doi.org/10.1016/j.ceramint.2020.07.145

Reference: CERI 25899

To appear in: *Ceramics International*

Received Date: 20 May 2020

Revised Date: 7 July 2020

Accepted Date: 14 July 2020

Please cite this article as: M. Starykevich, A. Jamale, F.M.B. Marques, Assessment of bismuth oxide-based electrolytes for composite gas separation membranes, *Ceramics International* (2020), doi: https://doi.org/10.1016/j.ceramint.2020.07.145.

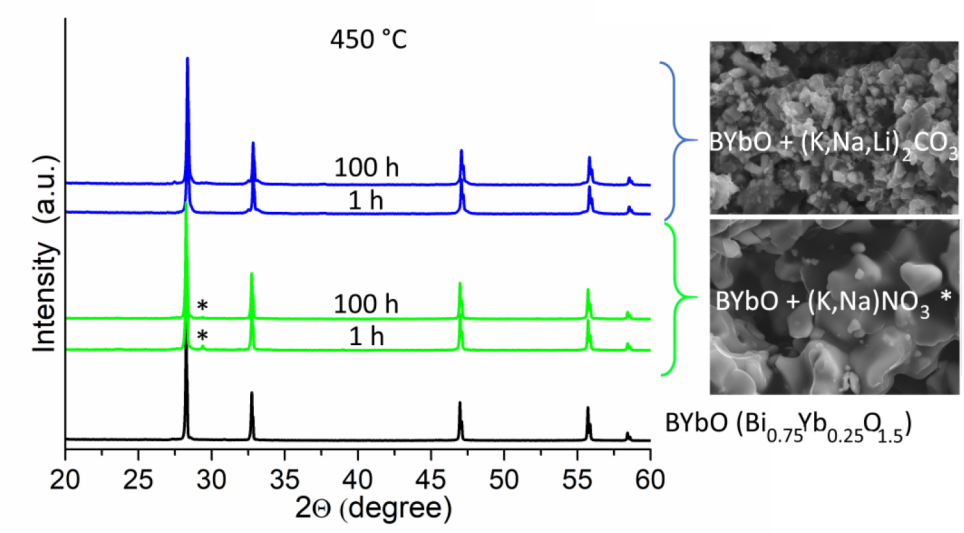

Assessment of bismuth oxide-based electrolytes for composite gas separation membranes

M. Starykevich[a,*], A. Jamale[a], F.M.B. Marques[a,b]

[a] *CICECO-Aveiro Institute of Materials, Department of Materials and Ceramic Engineering, University of Aveiro, 3810-193 Aveiro, Portugal*

[b] *Department of Materials Science and Engineering, UFPB – Federal University of Paraíba, 58051-900 João Pessoa, Brazil*

Abstract

Oxide+salt composites can be used in CO_2 and NO_x separation membranes, where high oxide-ion conductivity is crucial to improve performance. Pursuing this goal, the stability of three different bismuth oxide-based electrolytes (Cu+V, Y and Yb-doped) against molten alkali carbonates (Li, Na, K) or nitrates (Na, K) was tested firing them in the 450-550 °C temperature range, and with endurance tests up to 100 h. A well-known ceria-based composite was used as reference (CGO - $Ce_{0.9}Gd_{0.1}O_{1.95}$). Oxides and composites were studied by X-ray diffraction, scanning electron microscopy and impedance spectroscopy (in air, 140–650 °C temperature range). $Bi_2Cu_{0.10}V_{0.90}O_{5.35}$ easily reacts with molten salts. $Bi_{0.75}Y_{0.25}O_{1.5}$ and $Bi_{0.75}Yb_{0.25}O_{1.5}$ have higher stability against molten carbonates and complete stability against molten nitrates. The Y-doped oxide stability against the molten carbonates was enhanced changing the molten salt composition (Y_2O_3 additions) and using lower firing temperatures. Above all, composites based on Y or Yb-doped Bi_2O_3 with molten alkali nitrates showed impressive 6× or 3× higher electrical conductivity at 290 °C, in air (4.88×10^{-2} and 2.41×10^{-2} $S.cm^{-1}$, respectively) than CGO-based composites (7.72×10^{-3} $S.cm^{-1}$), qualifying as promising materials for NO_x separation membranes.

Keywords: Gas separation membranes; bismuth oxide; molten alkali carbonates; molten alkali nitrates; reactivity; impedance spectroscopy.

* Corresponding author. Tel.: +351 932433827
E-mail address: mstarykevich@ua.pt (Dr. M. Starykevich)

[b] Visiting Professor

Highlights

- Bi-based ceramic electrolytes show high stability in contact with molten nitrates
- Suitable dopants (oxide and/or salt) enhance the stability of Bi-based ceramics against molten alkali carbonates
- Bi-based composites (ceramic+alkali nitrates) show higher conductivity than state of the art ceria-based composites
- Y or Yb-doped Bi_2O_3 are promising candidates for NO_x separation membranes

Introduction

Greenhouse gas emissions and climate changes are central concerns threatening a sustainable development. Gas separation is an extremely important and fast developing scientific and industrial area aiming at removal of gas pollutant emissions. The high ion-based selectivity of electrochemical processes is uniquely suited for these purposes.

In the last decade composite CO_2 separation membranes (molten salt within an oxide skeleton) showed promising results [1-4], with tolerance to temperatures typical of some exhaust combustion gases. More recently, NO_x separation membranes were introduced by Zhang et al. [5], extending the field of composite membranes to the removal of the nitrogen oxides from gas mixtures, again a crucial environmental issue. In both cases the membrane should provide easy pathways for a variety of charge carriers, depending on the specific application.

CO_2 separation membranes include a solid oxide (SO) ion conductor (ceramic skeleton), and molten carbonates (MC) as providers of carbonate-ion transport (either directly or based on counter transport of alkali metal ions and neutral alkali carbonate molecules). CO_2 combines with O^{2-} (forming CO_3^{2-}) on the membrane feed side, while on the permeate side this process is reversed. Ambipolar conduction is needed inside the membrane, with O^{2-} transport proceeding in the opposite direction of net CO_3^{2-} transport [1, 6]. The phase distribution in composite membranes is schematically presented in Figure 1 while the role of each phase and surface reactions are described in Table 1. These composites depend strongly on the ceramic phase oxide-ion conductivity, which is rate determining for typical ceramic and molten salt ionic conductivity values and working temperatures in the 400-600 °C range [7-9].

NO_x membranes are based on a ceramic substrate with mixed oxygen-ionic and electronic conductivity (MIEC) and molten nitrates (MN). As alternative, an oxide-ion conductor can also be combined with an electronic conductor (EC), besides the salt phase. The working principle is slightly more complex due to extra electrons needed to compensate distinct ionic charges involved. Reaction of NO_x with oxygen (or O^{2-}) to yield NO_{x+1}^- must be balanced with release of an electron (e^-) in the membrane feed side, with an opposite reaction in the permeate side. Presence of oxygen in the feed side might generate a parallel transport of this species besides NO_x, with the exact oxygen flow depending on the oxygen activity gradient across the membrane [5]. Complete NO_x separation can be achieved with an additional oxygen separation membrane, yielding oxygen as side product. The phase

arrangement is again presented in Figure 1, while the role of phases and surface reactions are described in Table 1.

Table 1. Membrane types (see Figure 1), composition, surface reactions and inner charge transport in composite gas separation membranes.

Type		Materials			Feed side net surface reaction	Inner net charge transport	Ref.
Gas	Scheme	Salt	Oxide	Others			
CO_2	Fig. 1(1)	M_2CO_3[(1)]	SO[(2)]	None	$CO_2 + O^{2-} = CO_3^{2-}$	CO_3^{2-} and O^{2-}	[3, 4, 6]
NO_x	Fig. 1(2)	MNO_3 (MNO_2)[(3)]	MIEC[(4)]	None	$NO_x + O^{2-} = NO_{x+1}^- + e^-$	NO_{x+1}^-, O^{2-} and e^-	[5]
NO_x	Fig. 1(3)		SO	EC[(5)]			

[(1)] M corresponds to an alkali metal (e.g., Na, Li or K), but eutectic salt mixtures are often used to lower operating temperatures; [(2)] solid oxide-ion conductor; [(3)] at each temperature the exact salt composition is a result of the thermodynamic equilibrium between salt and gas phase species involved (e.g., NO, NO_2, O_2); [(4)] mixed (oxide) ionic and electronic conductor; [(5)] electronic conductor (ceramic or metal).

With typical molten salt ionic conductivities far above those reported for standard ceramic oxide-ion conductors [7-9], the search for improved membrane performance must rely on a judicious optimization of phase content and microstructures, and utilization of premium oxide-ion conductors. Bismuth oxide-based materials show extremely high oxide-ion conductivity at comparatively low temperature, as such being the obvious candidates. For instance, $Bi_2Cu_{0.1}V_{0.9}O_{5.35}$ has an ionic conductivity of ~1 mS/cm at 300 °C [10], which is 50-100 times higher than common O^{2-} conductors (CGO-Gd-doped ceria, $(La,Sr)(Ga,Mg)O_3$, or even yttria stabilized zirconia). However, the application of Bi-based materials seems limited by high reactivity with common alkali carbonate eutectic compositions. As a consequence, published literature on bismuth oxide-based materials for CO_2 separation membranes is scarce. For instance, a $Bi_{1.5}Y_{0.3}Sm_{0.2}O_3$ (BYS)/ternary carbonate eutectic system was used by Li et al. [11]. The permeation fluxes reached only 6.50×10^{-3}-6.60×10^{-2} $ml.cm^{-2}.min^{-1}$ in the 500-650 ^oC temperature range. Unfortunately, the exact membrane stability is unknown.

Rui et al. [12] used BYS as skeleton but part of the channel in the skeleton was covered by γ-Al_2O_3 in order to increase wettability by the molten salt. Permeation rates of 6.50×10^{-3} $ml.cm^{-2}.min^{-1}$ were obtained at 500 °C. Additionally, it was shown that when holding the BYS membrane at 650 °C, the flux increased from 0.026 to 0.066 $ml.cm^{-2}.min^{-1}$, situation ascribed to the rhombohedral (low conductivity)-fluorite (high conductivity) BYS

phase transition. This surprising result was explained by the known increased stability of the fluorite phase at high temperature [13, 14]. Again, signs of reactivity between the Bi-based material and the molten carbonates were not reported. However, alumina particles covering (at least partly) BYS might act as coating, preventing direct contact of BYS with the molten phase.

Dong et al. [15] used an asymmetric ceramic-carbonate dual phase membrane where ceria was mixed with the salt eutectic composition, and BYS was used as non-wetting support. Permeation at 900 °C reached 1.56 $ml.cm^{-2}.min^{-1}$. Finally, BYS was also used with samarium doped ceria as a non-wetting support for dual phase membranes [16]. The high stability of the CO_2 permeation flux (0.18-0.88 $ml.cm^{-2}.min^{-1}$ at 550−700 °C) for more than 160 h was demonstrated. In this system there was again no direct contact between the molten carbonates and BYS. In all these examples coatings (alumina) or a comparatively lower conductivity ceria-based electrolyte were limiting the membrane performance, reaching well below what might be predicted for Bi-based oxides [6].

Irrespective of the expected advantage of Bi-based oxides as composite membrane scaffolds, distinct oxide compositions were never screened with respect to basic aspects like reactivity and electrical conductivity. Thus, this work addresses the possible use of three Bi-based oxides as ceramic skeletons for gas separation membranes. Nominal $Bi_2Cu_{0.10}V_{0.90}O_{5.35}$ (BICUVOX), $Bi_{0.75}Y_{0.25}O_{1.5}$ (BYO) and $Bi_{0.75}Yb_{0.25}O_{1.5}$ (BYbO) were selected for tests. BICUVOX and BYO are obvious options since they possess a high oxide-ion conductivity at low temperature (42 and 26 $mS.cm^{-1}$ at 500 °C correspondingly [10, 14]). BYbO has moderate ionic conductivity at low temperature (13 $mS.cm^{-1}$ at 500 °C [17]). However, besides this, Yb_2O_3 is quite stable in contact with alkali carbonate eutectic compositions up to 700 °C [18], an interesting feature deserving proper assessment.

With respect to the selection of molten salts, up to now large attention was dedicated to the Na_2CO_3 + Li_2CO_3 (NLC) eutectic composition [2-4, 6, 18]. Here the ternary carbonate eutectic (including also K_2CO_3, KNLC) will be considered as molten phase because of a much lower melting temperature (around 400 °C) with respect to NLC (500 °C) [8]. This advantage coupled with a high oxide-ion conductivity of the skeleton at low temperature should allow a lower membrane working temperature with high permeability. Additionally, the same skeleton materials will be tested as candidates for NO_x separation membranes, using KNN as molten phase (KNO_3 + $NaNO_3$ eutectic composition, melting at 238 °C only), allowing membrane operating temperatures as low as 250-300 °C [19]. While part of a materials screening procedure, emphasis in this study will be dedicated to the chemical

stability between phases (including endurance tests) and electrical conductivity. CGO will be used as reference composite ceramic matrix to benchmark the performance of these new Bi-based composites [4, 20].

2. Experimental

Bismuth oxide (Bi_2O_3, >99.5%, Riedel-de Haen), yttrium oxide (Y_2O_3, 99.99%, Aldrich), ytterbium oxide (Yb_2O_3, 99.9%, Alfa Aesar) vanadium oxide (V_2O_5, >99.0%, Fluka), copper oxide (CuO, for analysis, Merck), Gd-doped ceria (CGO, $Ce_{0.9}Gd_{0.1}O_{1.95}$, 99.9%, average particle size <200 nm, Praxair), potassium carbonate (KC, K_2CO_3, >99.0%, Sigma-Aldrich), sodium carbonate (NC, Na_2CO_3, >99.0%, Sigma-Aldrich), lithium carbonate (LC, Li_2CO_3, >99.0%, Sigma-Aldrich), potassium nitrate (KN, KNO_3, >99.0%, Sigma-Aldrich), and sodium nitrate (NN, $NaNO_3$, >99.0%, Sigma-Aldrich), were used as precursors.

$Bi_{0.75}Y_{0.25}O_{1.5}$, $Bi_{0.75}Yb_{0.25}O_{1.5}$ and $Bi_2Cu_{0.10}V_{0.90}O_{5.35}$ were synthesized by a classical solid state route [21, 22]. For the synthesis of BYO and BYbO, Y_2O_3 and Yb_2O_3 were calcined at 1000 °C for 2 h before weighing the powders. A simple mortar was used to mix the initial components and to hand grind the powder between consecutive firings (700 °C for 5 h and 750 °C for 10 h, respectively). The heating and cooling rates were 5 °C.min^{-1} for both stages. X-ray diffraction (XRD) showed, that after two firings, single phase fluorite structures were obtained. The synthesis of BICUVOX was done in three stages (500, 600, 700 °C for 5, 5 and 12 h respectively). The heating and cooling rates were also 5 °C.min^{-1}. The mixture of initial powders (Bi_2O_3, V_2O_5 and CuO) and intermediate grinding were again performed in a mortar. XRD confirmed the presence of only one phase.

KNLC was prepared by mixing KC, NC and LC in a 25.0, 31.5 and 43.5 mol% ratio [8], respectively, while KNN was prepared by mixing KN and NN in a 56.0:44.0 mol% ratio [19], respectively using in both cases high energy ball milling at 650 rpm, for 30 min. These compositions were stored in a desiccator and used for dosage with the oxides without any additional treatment.

A mortar was used again to mix the distinct ceramic phases and the salts in a 50:50 and 70:30 vol% ratio, for reactivity and electrical conductivity tests, respectively. The powders were uniaxially pressed (100 MPa) as disks with 8 mm in diameter and about 1.5-2 mm thick, before firing.

A high vol% of both phases (50:50 vol%) results in an easier detection of new products in reactivity tests performed in air in three sets of (temperature/time) conditions. The first tests were done at 450 °C for 1 h. This temperature is slightly higher than the melting point of KNLC (400 °C). The second test (long-term), was also performed at 450 °C but during 100 h. The last test, exploiting accelerated degradation conditions, was done at 550 °C

for 1 h. Notwithstanding the fact that the melting point of KNN is much lower than for KNLC, all reactivity tests were performed in the same conditions.

Samples for electrical conductivity measurements were also isostatically pressed at 200 MPa before sintering at 550 °C (5 °C.min^{-1} heating-cooling rate) for 1 h (except when mentioned in the text). Electrochemical measurements were performed using an HP 4284A LCR Meter with ac signal amplitude of 0.5 V (rms) within the 20 Hz to 1 MHz frequency range (with 10 points per decade). Prior to the electrical measurements, samples were painted with Au paste and the electrodes fired in air at 550 °C (3 °C.min^{-1} heating-cooling rate) for 10 min. Gold wires were used as current collectors, with all measurements performed in air within the 140–650 °C temperature range.

Investigation of the composites microstructure was performed using a Hitachi SU-70 scanning electron microscope (SEM) coupled with energy dispersive spectroscopy (EDS, Bruker Quantax 400 detector). XRD of all samples was performed at room temperature using a PANalytical XPert MPD PRO diffractometer (Ni-filter, CuKα radiation, PIXcel^{1D} detector, and exposition corresponding to about 200 s per step of 0.02 ° over 10–80 ° 2θ), at room temperature.

3. Results and discussion

3.1 Reactivity

Figure 2a shows typical XRD patterns of the initial powders before reactivity tests. It is clearly seen that initial ceramic powders are single phase, corresponding to $Bi_{0.75}Y_{0.25}O_{1.5}$, $Bi_{0.75}Yb_{0.25}O_{1.5}$ and $Bi_2Cu_{0.10}V_{0.90}O_{5.35}$ (see Table 2). The salt eutectic mixture patterns include several peaks that can be ascribed to distinct phases, including precursor salts and compounds (mixed salts) formed during high energy milling. Mixed salts are easily formed by mechanochemical synthesis, as previously reported [23]. For this reason, a cumbersome indexation of peaks was skipped in this case. Even with these limitations, main peaks in KNLC and KNN precursor patterns facilitate phase identification after reactivity tests. All phases detected in the systems after firing are summarized in Table 2.

The first oxide/salt couple investigated was BICUVOX/KNLC. During reactivity tests, BICUVOX showed substantial degradation with formation of new phases already at 450 °C after 1 h only. At 450 °C/100 h extensive structural changes can be noticed, more than observed at 550 °C/1 h (Figure 2b). Longer reaction times result in the formation of an undesirable specific cubic bismuth oxide symmetry (lower conductivity). Decomposition of BICUVOX could occur with formation of bismuth and vanadium compounds (e.g., oxides,

orthovanadates [24, 25]), but there is no evidence for the presence of vanadium related compounds. In fact, these systems include an additional difficulty resulting from the presence of significant amounts of amorphous phases formed during cooling of the molten phase. This will become evident during the analysis of microstructures. In these circumstances distinct cations can be dissolved in the abundant molten phase without formation of crystalline compounds. From these tests, BICUVOX revealed a modest potential as ceramic skeleton for composites with molten KNLC.

Table 2. Summary of phases detected by XRD and corresponding International Centre for Diffraction Data (ICDD) Powder Diffraction Files (PDF). For salt mixtures, files corresponding to best peak matches are listed.

Peak	Compound	Crystalline structure	PDF
1	Bismuth Ytterbium Oxide	Cubic, Fm-3m (225)	04-013-0015
2	Bismuth Yttrium Oxide		00-040-0320
3	Copper Bismuth Vanadium Oxide	Tetragonal, I4/mmm (139)	04-015-0753
4	"KNLC"		
	Potassium Lithium Carbonate	Monoclinic, P21/c (14)	04-009-6084
	Lithium Sodium Carbonate	Anorthic, P1 (1)	04-011-4058
5	"KNN"		
	Sodium Nitrate	Rhombohedral, R-3c (167)	04-007-5272
	Potassium Nitrate	Orthorhombic, Pmcn (62)	01-071-1558
6	Bismuth Yttrium Oxide	Rhombohedral, R-3m (166)	00-040-1021
7	Bismuth Oxide	Cubic, Pn-3m (224)	04-015-0028
8	Bismuth Oxide	Cubic, I23 (197)	01-081-0563
9	Bismuth Vanadium Oxide	Monoclinic, C2/c (15)	01-077-4952
10	Bismuth Ytterbium Oxide	Orthorhombic, I	00-057-0113
11	Bismuth Oxide	Monoclinic, P21/c (14)	04-011-1986
12	Yttrium Oxide	Cubic, I213 (199)	04-019-6322

Nitrate eutectic mixtures look less reactive against BICUVOX, with the oxide preserving the initial structure after 1 h of testing at 450 °C (Figure 2c). Only after long-term testing and at higher temperature BICUVOX changes to monoclinic bismuth vanadium oxide. This secondary compound also has poor electrical transport properties. Hence, it was deliberately decided to remove this system from further tests.

The BYO/KNLC composite showed better stability when compared to the BICUVOX-based couple. The XRD analysis of BYO/KNLC treated at 450 °C for 1 h showed no changes in the structure of BYO (Figure 3a). Nevertheless, a longer exposure time (100 h) or higher temperature (550 °C) lead to formation of rhombohedral bismuth yttrium oxide (Figure 3a). This newly formed rhombohedral structure still has interesting oxide-ion conducting properties and can be a candidate for further investigation [26].

Bismuth yttrium oxide showed excellent stability with no structural changes after testing with KNN under all conditions (Figure 3b). This result clearly means that BYO is an interesting material for NO_x membranes.

Previous results obtained with BYO/KNLC justified a new set of experiments. In fact, yttrium oxide is used to stabilize the high temperature Bi_2O_3 fluorite phase [13, 14]. The cubic phase can be stable at room temperature only if the concentration of yttrium is higher than 25 at% (metal position). Accordingly, the BYO phase transition from cubic to rhombohedral (Figure 3a) can be explained by loss of yttrium, resulting in a sub-critical concentration in the skeleton material. The process can be schematically written as:

$$(1+x)\ Bi_{0.75}Y_{0.25}O_{1.5} + x/2\ M_2CO_3 = Bi_{0.75(1+x)}Y_{0.25(1-3x)}O_{1.5} + x\ MYO_2 + x/2\ CO_2 \quad (1)$$

with M being an alkali metal cation, $x<1/3$, and assuming that all KNLC alkali metal carbonates behave as reported for Li_2CO_3 in contact with Y_2O_3 in air at high temperature [27].

Yttrium losses from BYO were difficult to assess by XRD. Besides, patterns showed no evidence of other phases after reactivity tests. Anyhow, in order to avoid potential yttrium loss from BYO, Y_2O_3 was added to KNLC aiming at a change in the driving force for reaction (1). In line with this reasoning, mixtures of KNLC with 5 and 15 vol% Y_2O_3 showed a positive effect on the preservation of the crystalline structure of the scaffold (Figure 3c). In fact, the XRD pattern obtained from the KNLC sample with 5 vol% of Y_2O_3 showed partial stabilization of the cubic phase, even if with significant rhombohedral phase content. Increasing the Y_2O_3 concentration in KNLC to 15 vol% lowered rhombohedral BYO formation and enhanced the preservation of the initial fluorite structure.

Oxide additions to molten carbonates are effective solutions to change the acid-basic characteristics of the salt and improve the chemical compatibility against specific oxide phases. This procedure was extensively adopted in order to try to improve the stability of NiO as cathode material in Molten Carbonate Fuel Cells [28-30]. The positive impact of Y_2O_3

additions shown in Figure 3c indicates that the future design of similar composites might also exploit adjustments in the composition of the molten phase to increase the stability of the oxide.

The third composite, BYbO/KNLC, showed excellent stability at 450 °C. The XRD patterns (Figure 4a) obtained from the samples after short and long-term tests (1 h and 100 h, respectively) at 450 °C show only fluorite BYbO peaks and, additionally, some small peaks from the salt. However, exposure of the oxide to KNLC at higher temperature (550 °C) results in conversion of the initial BYbO fluorite phase to orthorhombic bismuth ytterbium oxide and monoclinic bismuth oxide (Figure 4a). Even with this temperature constraint, the potential of Yb-doped materials for CO_2 separation membranes exceeds clearly all other materials tested in this work.

Bismuth ytterbium oxide also showed excellent stability and no structural changes when exposed to KNN under all testing conditions (Figure 4b). This result also indicates that BYbO is an excellent candidate material for NO_x membranes.

3.2 Microstructure

SEM was used to inspect samples after extreme reactivity test conditions (550 °C/1 h). Figure 5 shows typical SEM images of cross sections of selected samples. Oxide particles appear light grey while a continuous dark grey region corresponds to the molten salt.

For BICUVOX-based composites, the usual ceramic skeleton flooded by a molten phase (KNLC) is hardly discerned, with the material consisting of large compacts where light grey sub micrometric particles are immersed in the formed molten phase (Figure 5a). The oxide particles seem to be homogeneously distributed with multiple contact points between them, suggesting a new phase formed by precipitation, after dissolution and decomposition of BICUVOX in the molten salt. Overall, these features are consistent with the reported BICUVOX high reactivity against KNLC and likely dissolution of copper and vanadium in the molten phase.

BYbO/KNLC, BYO/KNLC and BYO/KNN under the same conditions, also show complex microstructures (modest phase contrast in some regions) but with totally distinct features. Now oxide particles are clearly detached from the molten phase, (Figure 5b-d), situation consistent with the higher stability of the oxide phases during reactivity tests. The microstructure of CGO-based composites is skipped here since this issue was treated in detail in previous publications [31-33].

EDS mapping was also performed under slightly lower magnification to complement the above information on the characteristics of several samples (Figure 6). It is clearly seen that BICUVOX/KNLC has distinct bismuth and vanadium rich areas (Figure 6a). This confirms the high reactivity and decomposition of BICUVOX. On the contrary, elemental atomic mapping of BYO/KNLC and BYbO/KNLC demonstrates a higher consistency between the distribution of bismuth and dopant elements (Figure 6b through 6d). Only in the specific case where yttria was added to the salt mixture, local spots of Y can be observed besides the homogeneous distribution within the Bi-based phase (Figure 6d). In the three last cases, K mapping indicates that the corresponding specific areas tend to complement the oxide phase dominant areas (Figure 6b through 6d).

3.3 Electrochemical characterization

The electrochemical characterization of most systems was performed using impedance spectroscopy measurements in air. A typical set of results obtained for samples fired at 550 °C for 1 h, is shown in Figure 7a, including all oxide+KNLC composite materials. The main plot includes data obtained at 350 °C, when all phases are in the solid state. For the CGO-based composite, needing a distinct magnification, data is shown as left-hand side inset. Results obtained at 450 °C, with the salt already in the molten condition (about 50 °C above the melting point) are shown as a small inset (right hand side). At this last temperature the BICUVOX-based sample showed no mechanical integrity, preventing any measurement.

Results obtained with impedance spectroscopy measurements were consistent with the reactivity effects previously presented. BICUVOX evidenced extensive reaction with KNLC and the desirable mechanical stability of the ceramic skeleton vanished entirely under the setup light spring loading conditions. The remaining Bi-based electrolytes preserved their mechanical integrity even when some reaction occurred.

Analysis of impedance spectra assumed that the lower frequency tail corresponds to the electrode arc. Deconvolution of higher frequency spectra into distinct contributions was not even attempted. The composite nature of these materials is the source of mixed contributions of both phases and microstructure to the overall cell impedance. Common designations like bulk and grain boundary arcs make no sense in these circumstances even when the spectra somehow resemble typical polycrystalline ceramic electrolyte spectra. This issue was studied in great detail using CGO-based composites and further details are hereby skipped for this reason [23, 34].

From the relative magnitudes of composite impedances, the low temperature (350 °C) conductivity followed the sequence CGO>BYbO>BYO>BICUVOX, using the oxide phase designation to distinguish these composites. This result is in obvious contradiction with the relative conductivity of the ceramic phases, where BICUVOX is the best conductor and CGO the least conducting oxide phase. These results show the importance of reactivity and microstructure on the total conductivity. This issue will be addressed again during the analysis of temperature trends.

At higher temperature the composites conductivity merged to a smaller range of values with BYbO and BYO-based composites approaching the conductivity of the CGO-based composite, the latter still the best conductor. The relevance of the molten phase in these results is obvious, with KNLC acting as dominant charge carrier.

The limited stability of Bi-based electrolytes when in contact with KNLC at high temperature is confirmed with these results. The processing route adopted (joint milling and firing of both phases) offers a large surface area for oxide+salt reaction. Besides, impedance spectroscopy measurements involved an additional Au-electrode firing step (550 °C), and tests up to 650 °C. All these aspects influenced the reported modest electrical properties observed with these composites.

Complementary strategies are conceivable to avoid and/or decrease this problem. Initial consolidation of the ceramic skeleton before impregnation with the molten salt allows lower joint firing temperatures. In fact, impregnation of the skeleton can be obtained slightly above the salt eutectic temperature (around 400 °C), avoiding the 550 °C sintering step, thus decreasing the rate of reaction. As alternative, coating of a Bi-based ceramic skeleton with a thin ceria-based film (core-shell type of microstructure) could fully protect the core phase and enhance the wettability of the molten salt with respect to the oxide skeleton. This strategy is in line with previously reported attempts to coat Bi-based scaffolds.

Impedance spectroscopy results obtained with KNN are presented in Figure 7b. Again, data is grouped in two sets, the main plot corresponding to a temperature below melting (190 °C), and the inset corresponding to a temperature above melting (290 °C). Cell impedances now correspond to a conductivity trend BYO>BYbO>CGO, in close agreement with what might be expected from the conductivity of the oxide phases only.

While the relative conductivity magnitudes seem normal, looking at exact conductivity levels the results are surprising. The conductivity of all Bi-based composites exceeds significantly (minimum of one order of magnitude) the conductivity of the corresponding single-phase materials (oxides and salts) used as precursors. Table 3 lists

conductivity data values at 190 °C (this exact temperature is not available from all literature sources), to highlight this fact. Considerable scatter in literature data simply emphasizes the distinct nature and purity of samples but in all cases data values remain well below the results obtained in this work. Cases where extrapolation of high temperature data was used to estimate lower temperature data tend to be overestimated due to usual changes in activation energy with temperature observed in some of these materials. So, even when direct measurements are missing, the magnitudes of tabulated data offer and effective reference for comparison purposes.

Reasons for a conductivity enhancement in oxide+salt composites with respect to single phases are a source of debate for many years. Since comparison is between a composite with respect to nominally pure phases, the first issue deserving attention is on the potential cross doping between phases. Bi-based electrolytes are already doped materials, with compositions ideally adjusted to yield maximum conductivity levels. The solubility of alkali metal ions in the distinct Bi-based phases is unknown and only speculation based on size and coordination of potential dopants is viable. For a similar coordination (VI) Na^{+} and Bi^{3+} have comparable ionic radii but K^{+} is much larger [35]. On the contrary, the formation of $MBiO_3$ compounds (M-Li, Na, K) is well established, with Bi-ions forced to the pentavalent oxidation state [36]. These materials find promising applications as electrodes for alkali metal batteries only, but not as oxygen-ion conductors [37].

With respect to salt doping, the few results known indicate a negative effect on conductivity of salts with higher valence cations. Tests involving $NaNO_3$ doped with barium, nickel or chromium nitrates, showed always lower electrical conductivity. This was explained as a consequence of the annihilation of metal interstitial cations, assumed as dominant charge carriers [38]. This would be the expected (negative) result if some Bi^{3+} somehow acted as salt dopant.

Table 3. Conductivity of distinct single-phase materials and composites for gas separation membranes.

Material	T (°C)	σ (S.cm^{-1})	Sample	Data source	Ref.
NN	190	1.1×10^{-8}	polycrystalline	Plot	[39]
NN	190	1.8×10^{-10}	solution grown (sg)	Plot	[38]
NN	190	2.5×10^{-10}	melt grown (mg)	Plot	[38]
NN	190	1.6×10^{-9}	mg + cooled	Plot	[38]
NN	190	7.1×10^{-9}	polycrystalline	Plot	[38]
NN	190	4.5×10^{-8}	polycrystalline	plot	[40]
KN	190	7.9×10^{-8}	polycrystalline	plot	[39]
KN	190	4.1×10^{-7}	mg	plot (extrapol.)	[41]
KN	190	2.0×10^{-7}	single crystal	plot (extrapol.)	[41]
KN	190	2.0×10^{-7}	polycrystalline	plot	[40]
BYO fluorite	190	8.9×10^{-8}	polycrystalline	plot	this work
BYO rhomb.	190	1.4×10^{-8}	polycrystalline	plot (extrapol.)	[26]
BYO	190	2.0×10^{-6}	polycrystalline	plot (extrapol.)	[17]
BYbO	190	8.4×10^{-7}	polycrystalline	plot (extrapol.)	[17]
BYO/KNN	190	1.7×10^{-5}	composite	EIS	this work
BYbO/KNN	190	4.2×10^{-6}	composite	EIS	this work
CGO/KNN	190	2.5×10^{-6}	composite	EIS	this work

Unusual composite effects are known when salts and oxides are mixed, due to the formation of mobile metal vacancies accumulated in the space charge region adjacent to the oxide/salt interface [42-44]. Also, easy decomposition of these salts under mild thermal treatment, with easy formation of hydroxides after combination with the surrounding humidity, could explain the presence of molten phases at temperatures below the expected nitrate eutectic. Molten phases would easily explain enhanced conductivity at modest temperatures (e.g., KNO_3 and KOH mixtures have melting temperatures in the 210-220 °C range [45]). Whether or not similar phenomena could explain the observed conductivity enhancement in the present composites remains an open question. Since we are examining low temperature performance, below the target operating temperature of gas separation membranes, this discussion will be discontinued.

The high temperature spectra of all composites showed only an electrode arc, extending slightly to negative Z" values because of setup self-inductance. Even so, the high frequency (Z') intercept of these high-temperature spectra (Figure 7) allowed the determination of the total conductivity. Since the total conductivity is the sum of parallel contributions of skeleton and molten phase [33], the closer vicinity of all sets of data with respect to lower temperature data indicates again the dominant role of the molten salt in these higher temperature ranges.

Figure 8 shows typical Arrhenius-type (total) conductivity plots for the systems under investigation. The well-studied and stable CGO-based composites were also included as reference. Typical results at selected temperatures and activation energies (E_a) are presented in Table 4.

Figure 8a contains the results of KNLC based systems with all ceramic phases. As reference, a few extra lines were also introduced to show the exact performance of selected Bi-based oxide phases (BYO, fluorite structure [this work], and BYO, rhombohedral [26]). Figure 8a stresses why the BICUVOX/KNLC system was abandoned. Extremely low conductivity after reaction between the ceramic phase and the ternary eutectic is evident, besides the absence of higher temperature data due to mechanical collapse of the sample. For the remaining composites (CGO, BYO and BYbO-based), three regions are easily noticed, corresponding to the performance below the salt eutectic temperature, above the eutectic, and when the eutectic temperature is crossed.

At low temperature, before salt melting, all composites possess a relatively large activation energy for electrical conductivity. For the BYO/KNLC system this value is 107.3 $kJ.mol^{-1}$. This activation energy matches closely the activation energy of pure rhombohedral bismuth yttrium oxide (105.3 $kJ.mol^{-1}$) and is slightly smaller than observed for BYO with a fluorite-type structure (118.1 $kJ.mol^{-1}$). Due to the phase transition from fluorite to rhombohedral, the total conductivity of the composite is lower than observed for the CGO based membrane.

Conversion from the fluorite into the rhombohedral phase should impact the magnitude of the conductivity but should have a small effect with respect to activation energy. Core-shell like particles of BYO after interaction of the ceramic with KNLC are also possible, where the shell is rhombohedral and the core has a fluorite structure. These two layers could easily cooperate with respect to oxide-ion transport.

The BYbO/KNLC system shows a similar behavior. The activation energy at low temperature (105.8 $kJ.mol^{-1}$) correlates well with the corresponding values for other bismuth

oxide-based materials. The conductivity at low temperature is higher than observed for the BYO-based system, but not enough to compete with the CGO-based composite. Overall, since we have conflicting trends between the relative orders of magnitude of conductivity for all composites and for the ceramic phases only, reported reactivity and microstructural constraints cannot be ignored.

Table 4. Selected values of electrical conductivity (σ) and activation energy (E_a) at low ($E_{a,LT}$) and high temperatures ($E_{a,HT}$) obtained for distinct composites and for single phase Bi-based oxides.

Oxide	Salt	Firing T (°C)/t (h)	σ at 350 °C ($S.cm^{-1}$)	$E_{a,LT}$ ($kJ.mol^{-1}$)	σ at 450 °C ($S.cm^{-1}$)	$E_{a,HT}$ ($kJ.mol^{-1}$)
BYO fluorite	-	550 °C/1 h	1.42×10^{-4}	118.1	2.71×10^{-3}	-
BYO rhombohedral	-	550 °C/1 h	1.62×10^{-5} [26]	105.3	2.11×10^{-4} [26]	-
BYO	KNLC	550 °C/1 h	4.99×10^{-6}	107.3	1.11×10^{-2}	55.0
BYO	KNLC+Y_2O_3	550 °C/1 h	5.20×10^{-6}	109.2	2.63×10^{-3}	67.6
BYO	KNLC	450 °C/1 h	2.27×10^{-5}	116.6	9.37×10^{-3}	56.4
BICUVOX	KNLC	550 °C/1 h	1.08×10^{-6}	-	-	-
BYbO	KNLC	550 °C/1 h	1.70×10^{-5}	105.8	1.89×10^{-2}	48.3
CGO	KNLC	550 °C/1 h	1.80×10^{-4}	87.9	5.34×10^{-2}	41.4
		Firing T (°C)/t (h)	σ at 190 °C ($S.cm^{-1}$)	$E_{a,LT}$ ($kJ.mol^{-1}$)	σ at 290 °C ($S.cm^{-1}$)	$E_{a,HT}$ ($kJ.mol^{-1}$)
BYO	KNN	550 °C/1 h	1.66×10^{-5}	129. 8	4.88×10^{-2}	23.3
BYbO	KNN	550 °C/1 h	4.18×10^{-6}	117.1	2.41×10^{-2}	13.0
CGO	KNN	550 °C/1 h	2.45×19^{-6}	100.7	7.72×10^{-3}	19.2

The electrical conductivity results of the composite with 15 vol% yttrium oxide addition to KNLC are presented in Figure 8b. While the conductivity of the composite in the low temperature region is almost the same as without extra Y_2O_3 addition, the conductivity of the system at high temperature is lower than it was before. This conductivity drop can be explained by a decreasing amount of liquid phase due to partial combination of KNLC with the oxide addition and a likely drift in composition of the salt phase (e.g., formation of $LiYO_2$ with CO_2 release).

Due to the positive stability of cubic BYO when exposed to KNLC at 450 °C, it was also decided to try to sinter BYO/KNLC membranes only at 450 °C, for 1 h. The electrical conductivity results are presented in Figure 8b. The conductivity of this system is higher than for the remaining composites even if lacking proper densification of the pellet at lower

temperature. The activation energy calculated from the low temperature slope is 116.6 kJ.mol^{-1}. Since the activation energy of pure BYO, fluorite phase, is 118.1 kJ.mol^{-1}, the similarity suggests that cubic BYO prevails as oxide-ion conductor in the composite sintered at low temperature. This result confirmed that alternative processing routes (e.g., preliminary consolidation of the ceramic skeleton before impregnation) and lower operating temperatures can circumvent the reactivity problems.

At high temperature, above melting, the low activation energy of molten salts conductivity prevails. In between these two regions, close to the eutectic temperatures (398 °C =1.49×10^{-3} K^{-1} for KNLC or 238 °C =1.96×10^{-3} K^{-1} for KNN), huge step-like conductivity changes can be explained by the salt phase transition from solid to the molten state.

The results of conductivity measurements with composites for NO_x separation membranes, based on BYO and BYbO, are presented in Figure 8c. It is clear that the conductivity of the bismuth-based systems is always higher than found for the corresponding CGO-based composite. While the low temperature performance might indicate the relevance of oxide/salt interfacial conductivity effects, previously discussed, the high temperature conductivity trend clearly indicates the relevant role of the ceramic phase nature on the composite performance. These data confirm the superior characteristics of BYO and BYbO with respect to ceria-based electrolytes as scaffolds for NO_x separation membranes. Based on this preliminary materials screening, future work is planned to assess the impact of gas phase composition on the stability of the oxide phase in these composite materials.

4. Conclusions

Several Bi-based electrolytes tested for composite CO_2 separation membranes show a poor stability with respect to molten alkali metal carbonates. However, specific oxide dopants (e.g., Yb_2O_3), moderate working temperatures (up to 450 °C) and selected oxide additions (e.g., Y_2O_3) to the molten salt, can be used to circumvent these limitations. The stability of tested Bi-based oxides with respect to molten alkali nitrates seems fully consistent with their potential application in NO_x separation membranes, including chemical stability and electrical conductivity. Furthermore, total conductivity levels reached with these systems at potential working temperatures clearly exceed values obtained with the state-of-the-art ceria-based electrolytes.

Acknowledgements

This work was funded by projects CO2ZERO (POCI-01-0145- FEDER-016654 - PTDC /CTM -CER/6732/2014), MOCO3 - (M-ERA.NET2 2016 - MOCO3-0009/2016), and CICECO-Aveiro Institute of Materials, UIDB/50011/2020 & UIDP/50011/2020, financed by national funds through FCT (Fundação para a Ciência e a Tecnologia)/MCTES, and when applicable co-financed by FEDER under the COMPETE 2020 Program. Specific support (AJ) provided by national funds (OE), through FCT, IP, in the scope of the framework contract foreseen in the numbers 4, 5, and 6 of the article 23, of the Decree-Law 57/2016, of August 29, changed by Law 57/2017, of July 19.

5. References

[1] J.L. Wade, K.S. Lackner, A.C. West, Transport model for a high temperature, mixed conducting CO_2 separation membrane, Solid State Ionics, 178 (2007) 1530-1540. DOI: 10.1016/j.ssi.2007.09.007.

[2] J.L. Wade, C. Lee, A.C. West, K.S. Lackner, Composite electrolyte membranes for high temperature CO_2 separation, J. Membr. Sci., 369 (2011) 20-29. DOI: 10.1016/j.memsci.2010.10.053.

[3] H. Näfe, Electrochemical CO_2 separation through an alkali-carbonate-based membrane, ECS J. Solid State Sci. Technol., 3 (2014) N23-N29. DOI: 10.1149/2.003403jss.

[4] S.G. Patrício, E. Papaioannou, G. Zhang, I.S. Metcalfe, F.M.B. Marques, High performance composite CO_2 separation membranes, J. Membr. Sci., 471 (2014) 211-218. DOI: 10.1016/j.memsci.2014.08.007.

[5] G. Zhang, E.I. Papaioannou, I.S. Metcalfe, Selective, high-temperature permeation of nitrogen oxides using a supported molten salt membrane, Energy Environ. Sci., 8 (2015) 1220-1223. DOI: 10.1039/C4EE02256D.

[6] F.M.B. Marques, S.G. Patrício, E. Muccillo, R. Muccillo, On the model performance of composite CO_2 separation membranes, Electrochim. Acta, 210 (2016) 87-95. DOI: 10.1016/j.electacta.2016.05.141.

[7] M. Mizuhata, T. Ohashi, A.B. Béléké, Electrical conductivity and related properties of molten carbonates coexisting with ceria-based oxide powder for hybrid electrolyte, Int. J. Hydrogen Energy, 37 (2012) 19407-19416. DOI: 10.1016/j.ijhydene.2011.09.109.

[8] S. Frangini, A. Masi, Molten carbonates for advanced and sustainable energy applications: Part I. Revisiting molten carbonate properties from a sustainable viewpoint, Int. J. Hydrogen Energy, 41 (2016) 18739-18746. DOI: 10.1016/j.ijhydene.2015.12.073.

[9] V.V. Kharton, F.M.B. Marques, A. Atkinson, Transport properties of solid oxide electrolyte ceramics: a brief review, Solid State Ionics, 174 (2004) 135-149. DOI: 10.1016/j.ssi.2004.06.015.

[10] A.A. Yaremchenko, V.V. Kharton, E.N. Naumovich, F.M.B. Marques, Physicochemical and transport properties of BICUVOX-based ceramics, J. Electroceram., 4 (2000) 233-242. DOI: 10.1023/a:1009988531991.

[11] Y. Li, Z. Rui, C. Xia, M. Anderson, Y.S. Lin, Performance of ionic-conducting ceramic/carbonate composite material as solid oxide fuel cell electrolyte and CO_2 permeation membrane, Catal. Today, 148 (2009) 303-309. DOI: 10.1016/j.cattod.2009.08.009.

[12] Z. Rui, M. Anderson, Y. Li, Y.S. Lin, Ionic conducting ceramic and carbonate dual phase membranes for carbon dioxide separation, J. Membr. Sci., 417-418 (2012) 174-182. DOI: 10.1016/j.memsci.2012.06.030.

[13] T. Takahashi, H. Iwahara, T. Arao, High oxide ion conduction in sintered oxides of the system Bi_2O_3-Y_2O_3, J. Appl. Electrochem., 5 (1975) 187-195. DOI: 10.1007/bf01637268.

[14] N.M. Sammes, G.A. Tompsett, H. Näfe, F. Aldinger, Bismuth based oxide electrolytes - structure and ionic conductivity, J. Eur. Ceram. Soc., 19 (1999) 1801-1826. DOI: 10.1016/S0955-2219(99)00009-6.

[15] X. Dong, J. Ortiz Landeros, Y.S. Lin, An asymmetric tubular ceramic-carbonate dual phase membrane for high temperature CO_2 separation, Chem. Commun. (Cambridge, U. K.), 49 (2013) 9654-9656. DOI: 10.1039/C3CC45949G.

[16] B. Lu, Y.S. Lin, Asymmetric thin samarium doped cerium oxide–carbonate dual-phase membrane for carbon dioxide separation, Ind. Eng. Chem. Res., 53 (2014) 13459-13466. DOI: 10.1021/ie502094j.

[17] P. Shuk, H.D. Wiemhöfer, U. Guth, W. Göpel, M. Greenblatt, Oxide ion conducting solid electrolytes based on Bi_2O_3, Solid State Ionics, 89 (1996) 179-196. DOI: 10.1016/0167-2738(96)00348-7.

[18] F.J.A. Loureiro, S. Rajesh, F.M.L. Figueiredo, F.M.B. Marques, Stability of metal oxides against Li/Na carbonates in composite electrolytes, RSC Adv., 4 (2014) 59943-59952. DOI: 10.1039/C4RA11446A.

[19] R.W. Bradshaw, A review of the chemical and physical properties of molten alkali nitrate salts and their effect on materials used for solar central receivers, ECS Proceedings Volumes, 1987-7 (1987) 959-969. DOI: 10.1149/198707.0959pv.

[20] S.G. Patrício, E.I. Papaioannou, B.M. Ray, I.S. Metcalfe, F.M.B. Marques, Composite CO_2 separation membranes: Insights on kinetics and stability, J. Membr. Sci., 541 (2017) 253-261. DOI: 10.1016/j.memsci.2017.07.008.

[21] N.M. Bogdanovich, D.I. Bronin, G.K. Vdovin, I.Y. Yaroslavtsev, B.L. Kuzin, Effect of $Bi_{0.75}Y_{0.25}O_{1.5}$ electrolyte additive in collector layer to properties of bilayer composite cathodes of solid oxide fuel cells based on La(Sr)MnO_3 and La(Sr)Fe(Co)O_3 compounds, Russ. J. Electrochem., 45 (2009) 456-464. DOI: 10.1134/s1023193509040168.

[22] J.C. Boivin, C. Pirovano, G. Nowogrocki, G. Mairesse, P. Labrune, G. Lagrange, Electrode–electrolyte BIMEVOX system for moderate temperature oxygen separation, Solid State Ionics, 113-115 (1998) 639-651. DOI: 10.1016/S0167-2738(98)00330-0.

[23] A.S.V. Ferreira, C.M.C. Soares, F.M.H.L.R. Figueiredo, F.M.B. Marques, Intrinsic and extrinsic compositional effects in ceria/carbonate composite electrolytes for fuel cells, Int. J. Hydrogen Energy, 36 (2011) 3704-3711. DOI: 10.1016/j.ijhydene.2010.12.025.

[24] G.A. Kolta, I.F. Hewaidy, N.S. Felix, N.N. Girgis, Reactions between sodium carbonate and vanadium pentoxide, Thermochim. Acta, 6 (1973) 165-177. DOI: 10.1016/0040-6031(73)85023-3.

[25] D.A. Habboush, D.H. Kerridge, S.A. Tariq, Molten lithium carbonate—sodium carbonate—potassium carbonate eutectic: the reaction of group VB and VIB metal oxides and oxyanions, Thermochim. Acta, 28 (1979) 143-153. DOI: 10.1016/0040-6031(79)87013-6.

[26] A. Watanabe, T. Kikuchi, Cubic-hexagonal transformation of yttria-stabilized Σ-bismuth sesquioxide, $Bi_{2-2x}Y_{2x}O_3$ (x = 0.215 − 0.235), Solid State Ionics, 21 (1986) 287-291. DOI: 10.1016/0167-2738(86)90191-8.

[27] M. Yamauchi, Y. Itagaki, H. Aono, Y. Sadaoka, Reactivity and stability of rare earth oxide–Li_2CO_3 mixtures, J. Eur. Ceram. Soc., 28 (2008) 27-34. DOI: 10.1016/j.jeurceramsoc.2007.06.013.

[28] E. Antolini, The stability of molten carbonate fuel cell electrodes: A review of recent improvements, Appl. Energy, 88 (2011) 4274-4293. DOI: 10.1016/j.apenergy.2011.07.009.

[29] J.D. Doyon, NiO solubility in mixed alkali/alkaline earth carbonates, J. Electrochem. Soc., 134 (1987) 3035. DOI: 10.1149/1.2100335.

[30] K.-i. Ota, Y. Matsuda, K. Matsuzawa, S. Mitsushima, N. Kamiya, Effect of rare earth oxides for improvement of MCFC, J. Power Sources, 160 (2006) 811-815. DOI: 10.1016/j.jpowsour.2006.04.055.

[31] A.I.B. Rondão, S.G. Patrício, F.M.L. Figueiredo, F.M.B. Marques, Composite electrolytes for fuel cells: Long-term stability under variable atmosphere, Int. J. Hydrogen Energy, 39 (2014) 5460-5469. DOI: 10.1016/j.ijhydene.2013.12.125.

[32] S. Rajesh, D.A. Macedo, R.M. Nascimento, G.L. Souza, F.M.L. Figueiredo, F.M.B. Marques, One-step synthesis of composite electrolytes of Eu-doped ceria and alkali metal carbonates, Int. J. Hydrogen Energy, 38 (2013) 16539-16545. DOI: 10.1016/j.ijhydene.2013.05.090.

[33] A.I.B. Rondão, S.G. Patrício, F.M.L. Figueiredo, F.M.B. Marques, Impact of ceramic matrix functionality on composite electrolytes performance, Electrochim. Acta, 109 (2013) 701-709. DOI: 10.1016/j.electacta.2013.07.229.

[34] A.S.V. Ferreira, T. Saradha, F.L. Figueiredo, F.M.B. Marques, Compositional and microstructural effects in composite electrolytes for fuel cells, Int. J. Energy Res., 35 (2011) 1090-1099. DOI: 10.1002/er.1843.

[35] R. Shannon, Revised effective ionic radii and systematic studies of interatomic distances in halides and chalcogenides, Acta Crystallographica Section A, 32 (1976) 751-767. DOI: 10.1107/S0567739476001551.

[36] M. Mehring, From molecules to bismuth oxide-based materials: Potential homo- and heterometallic precursors and model compounds, Coord. Chem. Rev., 251 (2007) 974-1006. DOI: 10.1016/j.ccr.2006.06.005.

[37] M.-K. Kim, S.-H. Yu, A. Jin, J. Kim, I.-H. Ko, K.-S. Lee, J. Mun, Y.-E. Sung, Bismuth oxide as a high capacity anode material for sodium-ion batteries, Chem. Commun. (Cambridge, U. K.), 52 (2016) 11775-11778. DOI: 10.1039/C6CC06712C.

[38] C. Ramasastry, Y.V.G.S. Murti, N.F. Mott, Electrical conduction in sodium nitrate crystals, Proc. R. Soc. London, Ser. A, 305 (1968) 441-455. DOI: doi:10.1098/rspa.1968.0126.

[39] W.J. Davis, S.E. Rogers, A.R.J.P. Ubbelohde, Melting and crystal structure. The mechanism of melting of group I nitrates, Proc. R. Soc. London, Ser. A, 220 (1953) 14-24. DOI: doi:10.1098/rspa.1953.0168.

[40] L.G. Kolomin, P.I. Protsenko, Electrical conductivity of polycrystalline alkali nitrates in stable states and at phase transitions, Russ. Phys. J., 11 (1968) 105-109. DOI: 10.1007/BF00822477.

[41] A. Mansingh, A.M. Smith, Dielectric dispersion in the paraelectric phase of potassium nitrate, J. Phys. D: Appl. Phys., 4 (1971) 1792-1796. DOI: 10.1088/0022-3727/4/11/325.

[42] J.B. Wagner, Transport in compounds containing a dispersed second phase, Mater. Res. Bull., 15 (1980) 1691-1701. DOI: 10.1016/0025-5408(80)90187-7.

[43] J. Maier, Surface induced defects in the space charge region and the enhancement of ionic conductivity in two-phase systems, Phys. Status Solidi B, 123 (1984) K89-K91. DOI: 10.1002/pssb.2221230160.

[44] N. Vaidehi, R. Akila, A.K. Shukla, K.T. Jacob, Enhanced ionic conduction in dispersed solid electrolyte systems CaF_2-Al_2O_3 and CaF_2-CeO_2, Mater. Res. Bull., 21 (1986) 909-916. DOI: 10.1016/0025-5408(86)90128-5.

[45] G.J. Janz, R.P.T. Tomkins, Additional single and multi□component salt systems. electrical conductance, density, viscosity and surface tension data, J. Phys. Chem. Ref. Data, 12 (1983) 591-815. DOI: 10.1063/1.555693.

Captions:

Figure 1. Schematic representation of phases in CO_2 (1) and NO_x (2-3) gas separation membranes (SO-Solid oxide; MC – Molten carbonates; MN – Molten nitrates; MIEC – Mixed ionic and electronic conductor; EC – Electronic conductor). Transparency of a few particles is used to stress the 3D percolation of all phases. See Table 1 for additional details.

Figure 2. XRD patterns of: (a) – precursor composite materials; (b) and (c) - BICUVOX after reactivity with KNLC and KNN, respectively, at different temperature/time combinations. The three main peaks in each phase are indexed. Numbers correspond to phases listed in Table 2.

Figure 3. XRD patterns of BYO after reactivity testing with: (a) - KNLC; (b) - KNN (450 °C/1 h, 450 °C/100 h, 550 °C/1 h); (c) KNLC+Y_2O_3 (c) at 450 °C/1 h. The three main peaks in each phase are indexed. Numbers correspond to phases listed in Table 2.

Figure 4. XRD patterns of BYbO after reactivity testing with KNLC (a) and KNN (b) at different temperatures and time. The three main peaks in each phase are indexed. Numbers correspond to phases presented in Table 2.

Figure 5. Typical SEM micrographs of BICUVOX/KNLC, BYbO/KNLC and BYO/KNLC (a, b, c) and BYO/KNN (d) composites after reactivity testing at 550 °C for 1 h.

Figure 6. SEM micrographs and matching elemental EDS maps of KNLC-based composites after 1 h of reactivity testing at 550 °C.

Figure 7. Typical impedance spectra of: (a) KNLC-based systems at 350, 450 °C and (b) KNN-based systems at 190, 290 °C.

Figure 8. Arrhenius-type plots of: (a, b) KNLC-based and (c) KNN-based composites in air. The sintering conditions of composites were 550 °C for 1 h (a,c) or as detailed in (b). In (a) also shown data for single phase BYO with distinct structures (see text for details).

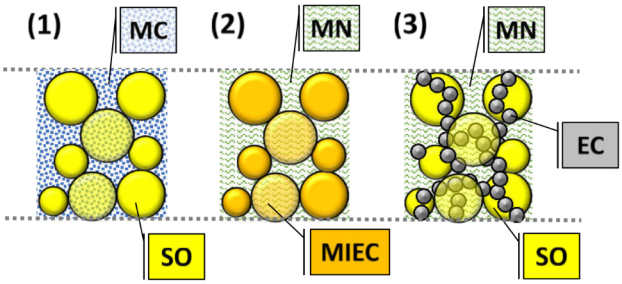

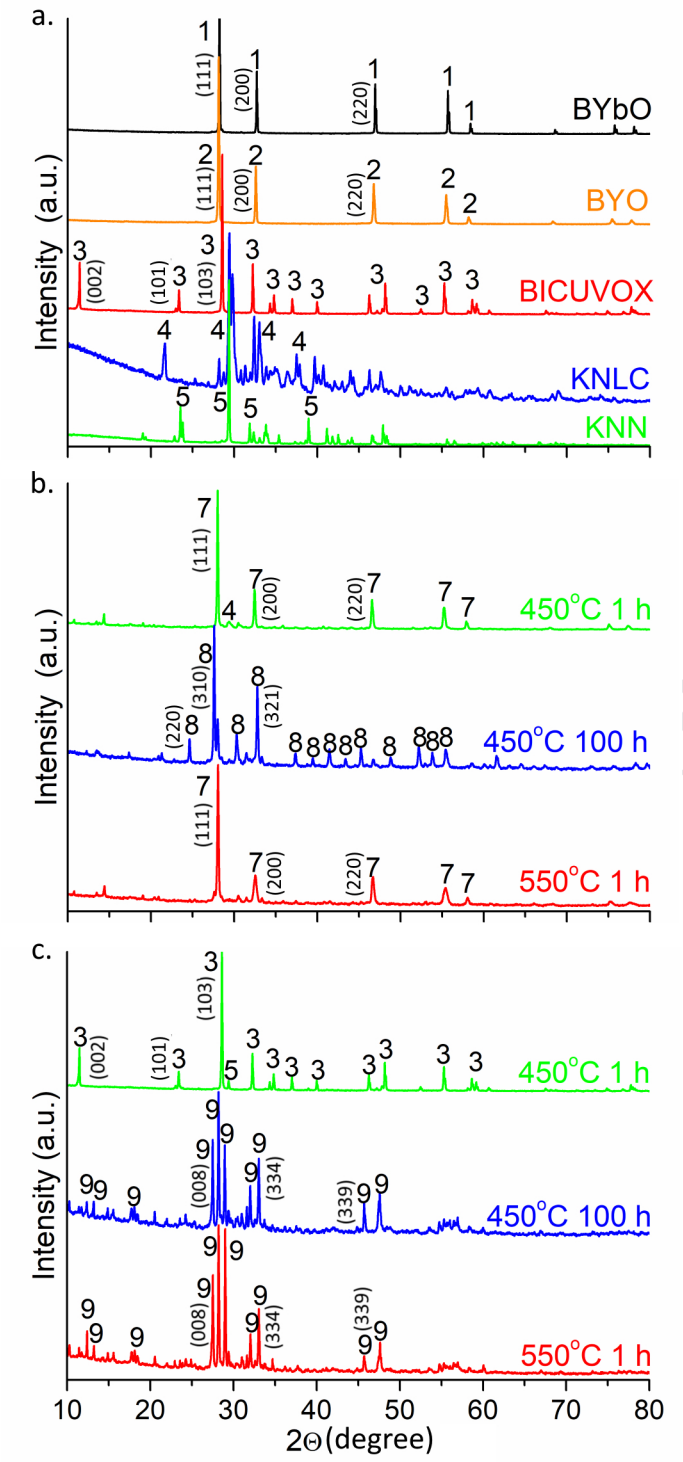
a.
BYbO
BYO
BICUVOX
KNLC
KNN
Intensity (a.u.)
b.
450°C 1 h
450°C 100 h
550°C 1 h
Intensity (a.u.)
c.
450°C 1 h
450°C 100 h
550°C 1 h
Intensity (a.u.)
2Θ(degree)

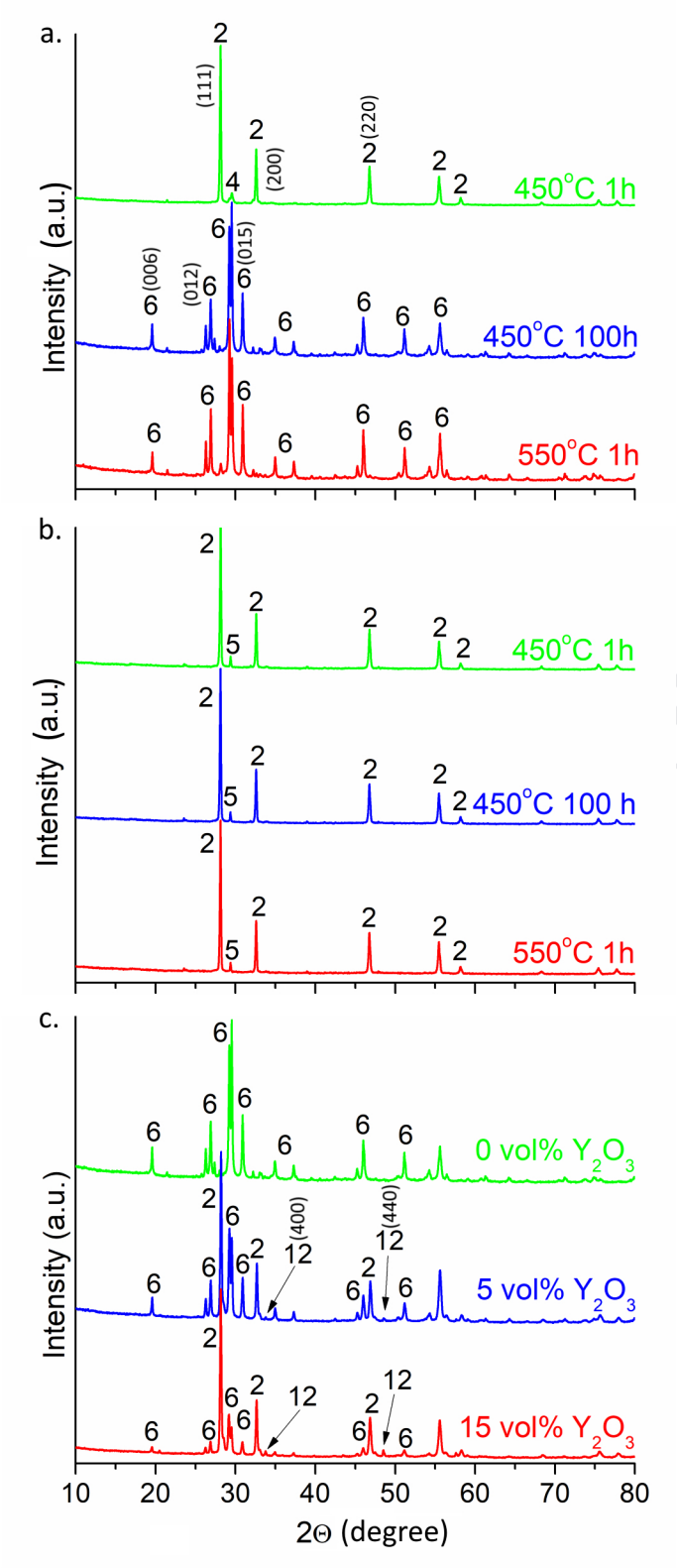
a.
b.
c.
Intensity (a.u.)
(111)
(200)
(220)
(006)
(012)
(015)
450°C 1h
450°C 100h
550°C 1h
450°C 100 h
0 vol% Y2O3
5 vol% Y2O3
15 vol% Y2O3
(400)
(440)
10
20
30
40
50
60
70
80
2Θ (degree)

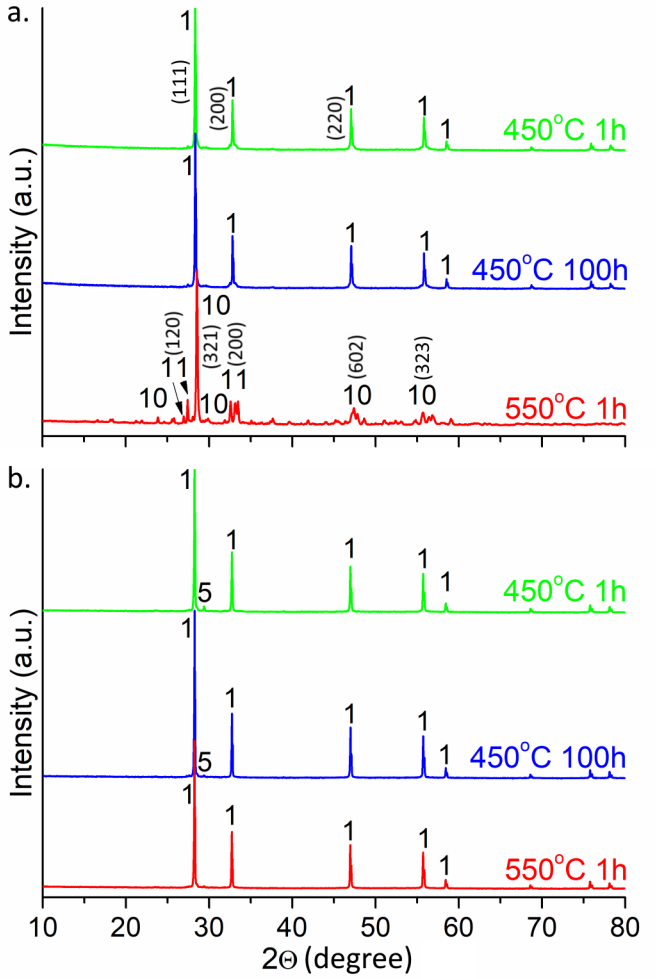

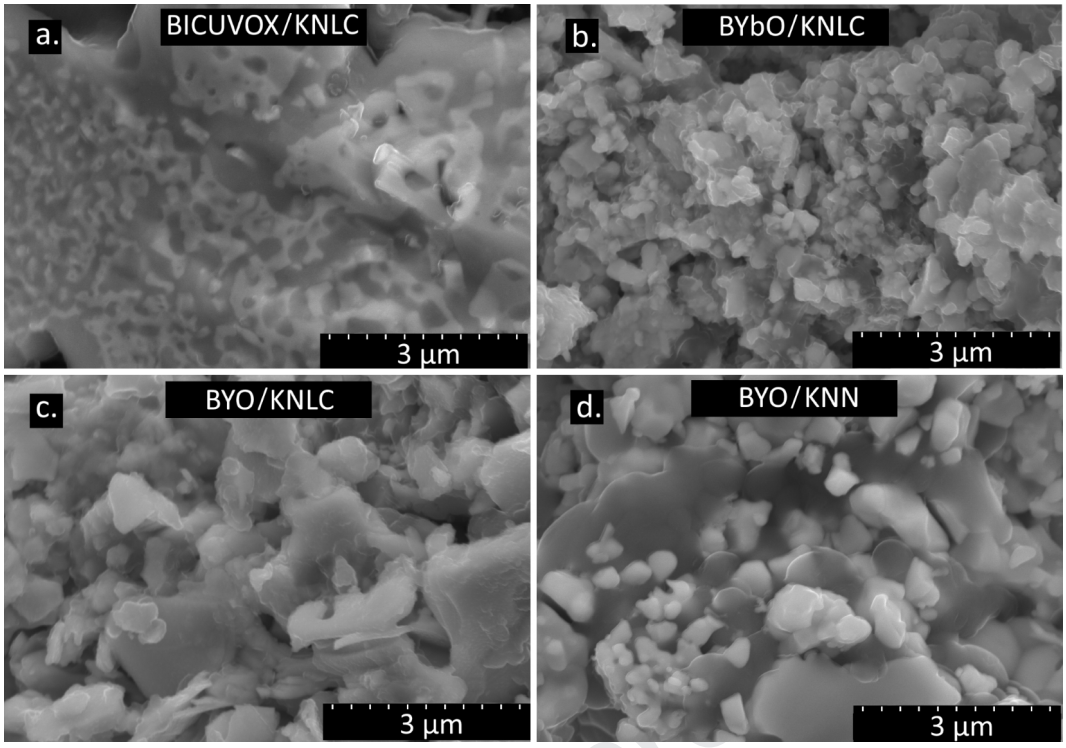

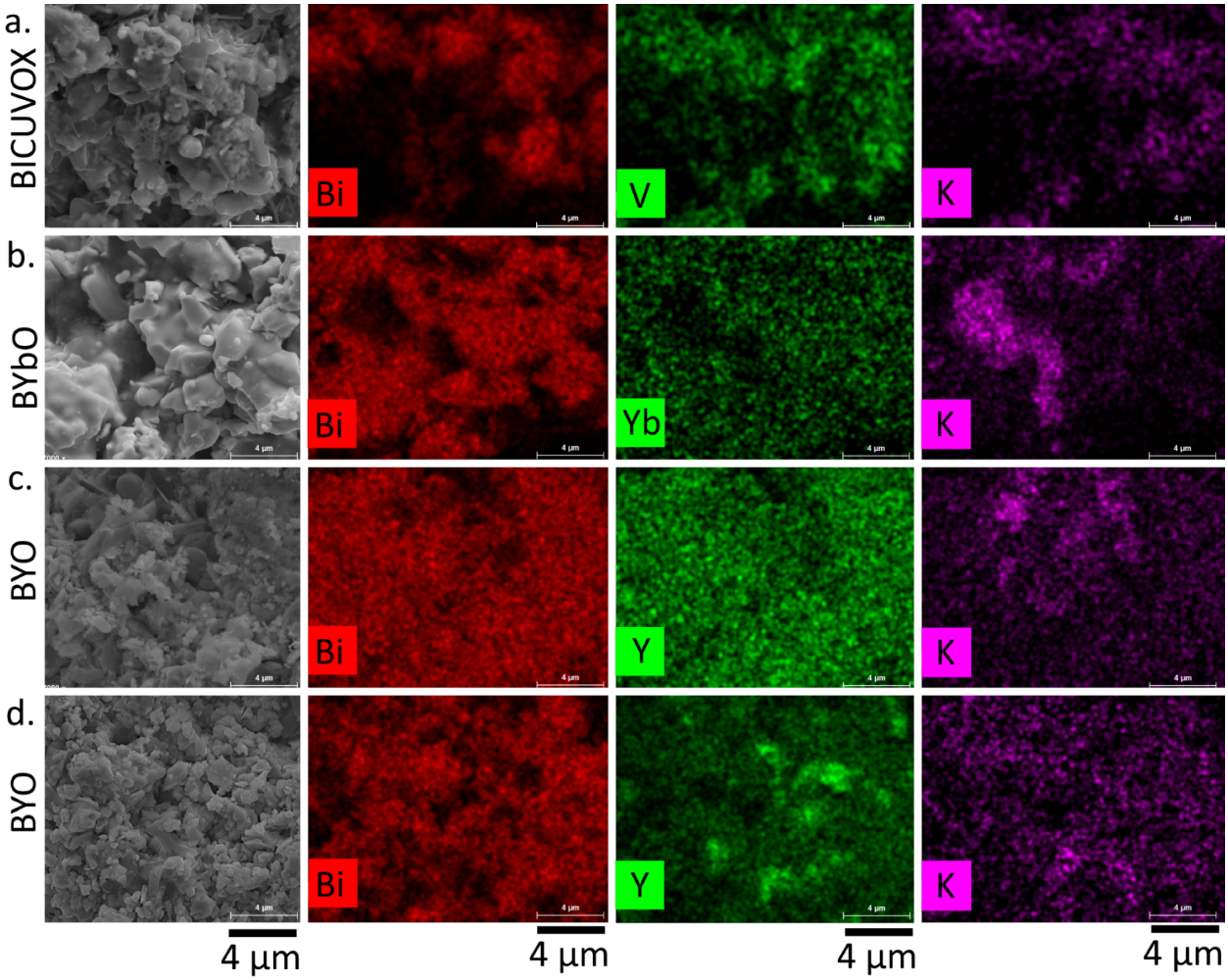
a.
BICUVOX
Bi
V
K
b.
BYbO
Bi
Yb
K
c.
BYO
Bi
Y
K
d.
BYO
Bi
Y
K
4 µm
4 µm
4 µm
4 µm

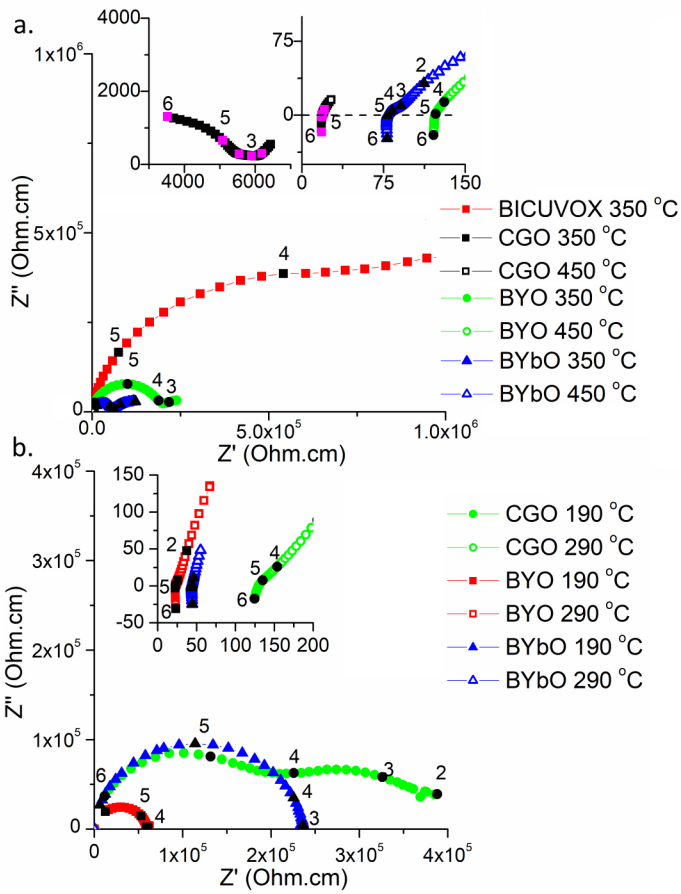

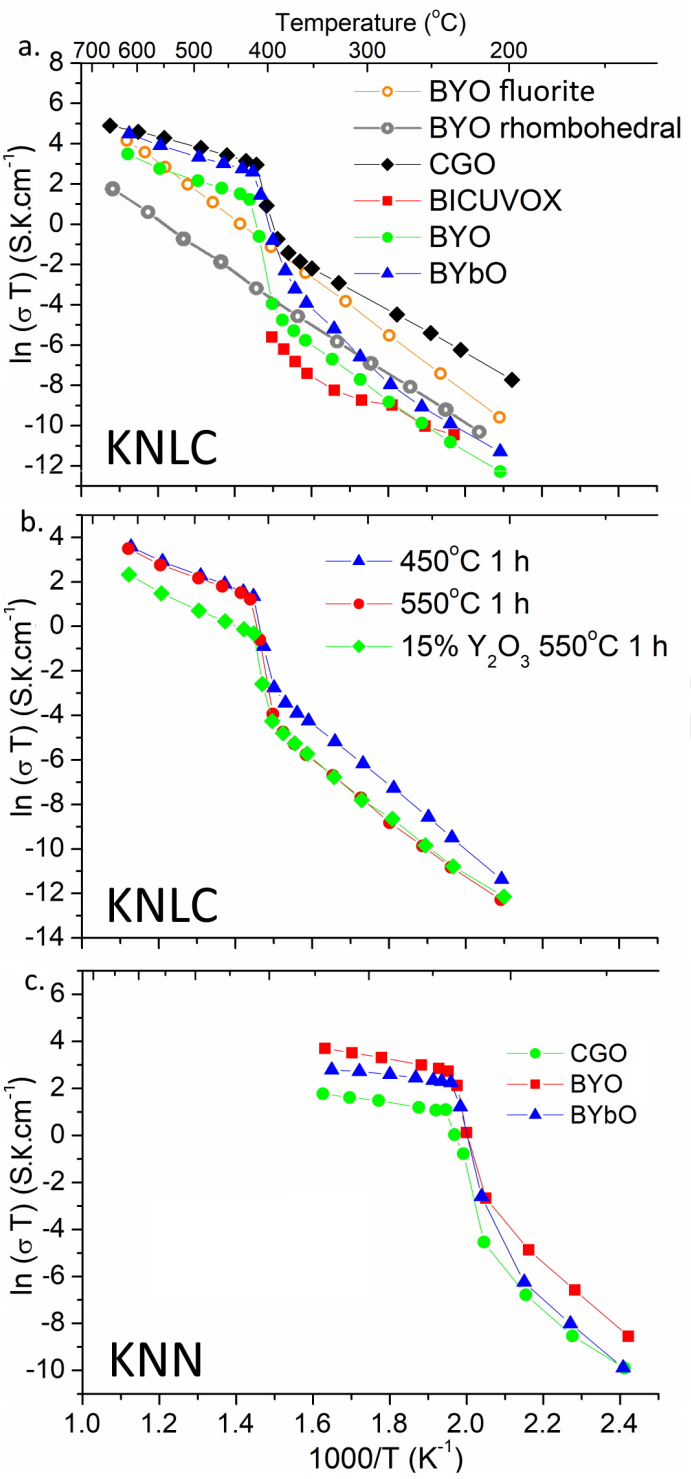
a.
Temperature (°C)
700 600 500 400 300 200
ln (σ T) (S.K.cm⁻¹)
BYO fluorite
BYO rhombohedral
CGO
BICUVOX
BYO
BYbO
KNLC
b.
450°C 1 h
550°C 1 h
15% Y2O3 550°C 1 h
KNLC
c.
CGO
BYO
BYbO
KNN
1000/T (K⁻¹)

Declaration of interests

☒ The authors declare that they have no known competing financial interests or personal relationships that could have appeared to influence the work reported in this paper.

☒The authors declare the following financial interests/personal relationships which may be considered as potential competing interests:

On behalf of authors team,
Dr. M.Starykevich.